J. H. Keller
R. G. Simmons

Sputtering Process Model of Deposition Rate

A model of the sputtering process has been developed that predicts the deposition rate of a sputtering system with parallel-plate geometry. By using data for sputtering yield vs voltage obtained from an ion-beam sputtering system, the model applies a new theory for computing the backscatter of the sputtered material, and, from the results, predicts deposition rates. The model also considers the effects of charge exchange in the sheaths, and of re-emission of sputtered material at the substrate. The model is valid for magnetic, tuned substrate, driven substrate, and controlled area ratio diode systems. Comparison with observed deposition rates shows good agreement for clean systems. An experimental APL *program that uses the model has been written.*

Introduction

In sputtering silicon dioxide and other dielectrics, the deposition rate is a function of power, target voltage, pressure, magnetic field, and wafer temperature, regardless of the sputtering system used. Both the deposition rate and the functional dependencies, however, differ from system to system. The differing deposition rates and observed functional dependencies given in, e.g., Refs. [1-5] point out the need for a consistent model for sputtering.

This paper describes a generalized model for sputtering systems, and a computer program that predicts the rate of deposition in a given system. In developing the model, data from the following system types have been used: magnetic field, tuned substrate, driven or biased substrate, and controlled area ratio diode systems. These systems are described in Refs. [1] and [6-9]. All are parallel plate types, and the study has been limited to SiO_2. Theoretical and empirical data for the effects of energy, backscatter of material, re-emission, and geometry have been incorporated into the model.

This paper is a detailed description of the "sputter transport and accumulation model" presented in Ref. [10]. We briefly describe the physics of the model; the derivations of the relationships involved in the program are given in Appendices A and B. Also, predicted and observed deposition rates are compared; curves of rate vs pressure, target voltage, and spacing are discussed. Finally we describe the experimental APL program written for use in calculating deposition rates. This interactive program prompts the user for a set of conditions as input, and then predicts the deposition rate for that set of conditions.

The model

The physical processes and the resultant parameters are as follows:

Physical process	*Resultant parameter*
1. Ions and energetic neutrals crossing the target dark space	Energy with which these particles strike the target
2. Emission of target material	Target sputtering rate
3. Transport of sputtered material from target to substrate, including backscattering by gas	Transmission coefficient
4. Re-emission of material from the substrate	Deposition rate and re-emission coefficient

These processes are illustrated in Fig. 1.

Particle energy

To determine the yield from the target, we must determine the energy distribution of the particles that strike the target. At low pressures, below 1.3 Pa (0.01 torr; 1 torr = 1.33×10^2 Pa), most of the particles are ions with energies close to that of the bias voltage across the target dark space. At high pressure, however, charge exchange plays an important role in reducing the mean energy per particle, while the total energy of all the particles remains nearly constant.

For ease of calculation, the particles that strike the target can be broken down into four groups:

1. Ions accelerated through the dark space without suffering collisions or charge exchange.
2. Ions formed somewhere in the dark space and then accelerated the remaining distance without suffering charge exchange. We will assume that these ions are produced by charge exchange.
3. Energetic neutral species produced by charge exchange with ions that originated in the plasma.
4. Energetic neutral species produced by secondary charge exchange in the dark space.

Having made this breakdown, one can compute the energy distribution as a function of pressure and dark space thickness. This computation is given in Appendix A.

The four groups are diagrammed in Fig. 2. The relation derived in Appendix A for the energy distribution of the particles times their energy E is given by

$$E(V) = eVN(V)$$

or

$$E(V) = \frac{J_o V d}{V_o \lambda_i}\left[2 + \frac{d}{\lambda_i}\left(1 - \frac{V}{V_o}\right)\right]\exp\left(-\frac{Vd}{V_o\lambda_i}\right) + J_o V_o \delta(V_o - V)\exp\left(-\frac{d}{\lambda_i}\right), \quad (1)$$

where V_o is the target bias voltage, d is the dark space thickness, δ is the Dirak delta function, e is the electron charge, V is the potential, N is the number density of particles, λ_i is the mean free path of ions, and J_o is the ion current density through the dark space. To show that the theory is reasonable, the energetic particle current predicted by Eq. (1) is compared to the ion current measured by a retarding potential instrument for a pressure-dark space thickness (pd) of about 7.3 Pa-cm (0.055 torr-cm) in Fig. 3.

The curve of the distribution of the energy of the particles $E(V)$ for a pd value of 7.3 Pa-cm (0.055 torr-cm) is shown in Fig. 4. This product corresponds to the operating conditions near 13 Pa (0.1 torr), zero magnetic field, and 13.56 MHz. As Fig. 4 shows, the mean energy per particle at this pressure is reduced to about 3/4 of the target bias voltage V_o.

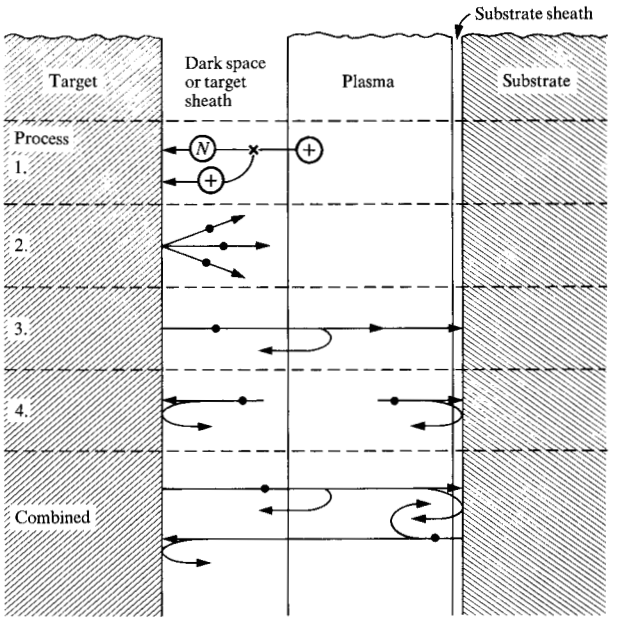

Figure 1 Physical processes of the sputtering model.

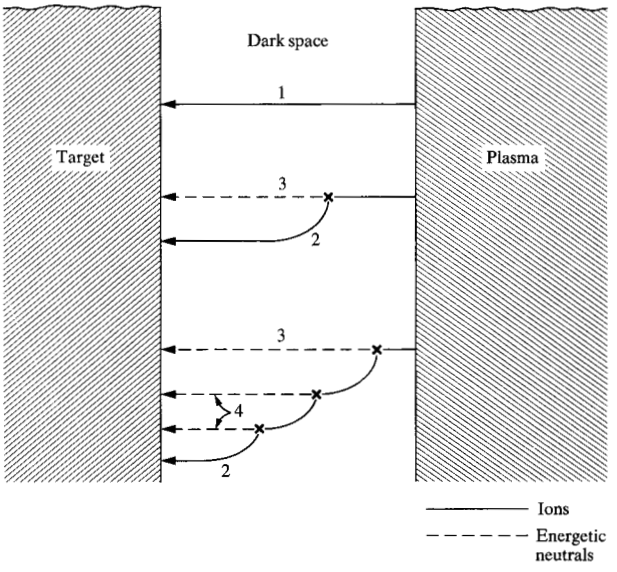

Figure 2 Energetic particles striking the target.

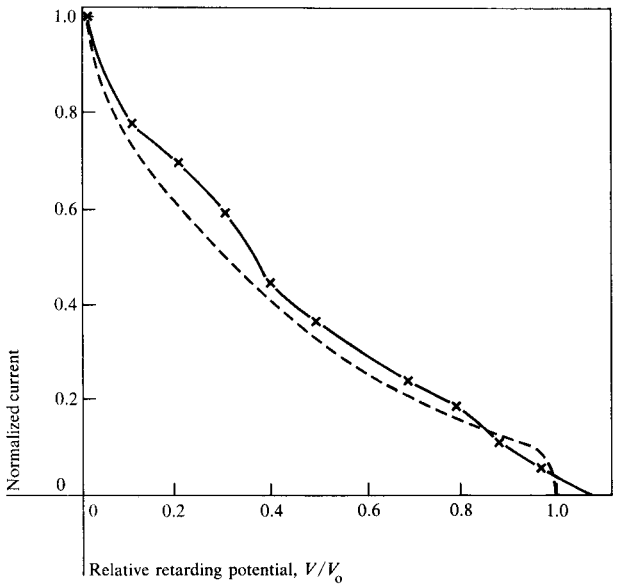

Figure 3 Theoretical energetic particle current (---) and experimental ion current (—) vs the relative retarding potential (V/V_0) ($pd \approx 7.3$ Pa-cm, 0.055 torr-cm).

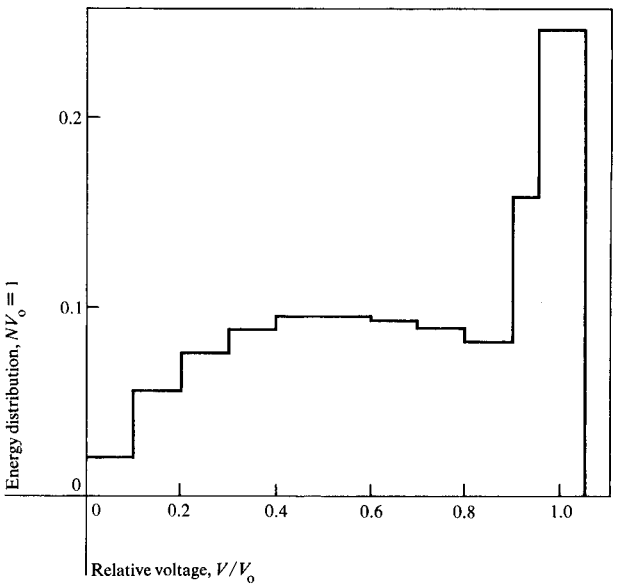

Figure 4 The energy distribution of particles vs the relative voltage (V/V_0) ($pd \approx 7.3$ Pa-cm, 0.055 torr-cm).

Target emission

Data on yield (molecules per ion) as a function of ion energy were obtained with a system that sputters dielectric materials with a neutralized ion beam of a given energy. In this way a curve of yield vs ion energy was obtained (Fig. 5). To put the data into a more useful form, the yield data were divided by the ion energy to give a curve of "yield efficiency," in molecules per keV of energy, vs the voltage of the sputtering argon ions (see Fig. 6). This curve shows an optimum sputtering energy somewhere between 300 and 800 eV.

To obtain a yield from a target in a sputtering system, we assume that the neutral argon particles sputter at the same rate as argon ions with the same energy. This assumption is borne out by the experimental data for metals, and by the currently accepted theories of the sputtering mechanism. Thus, by integrating the yield efficiency times the energy distribution of the particle flux that strikes the target, one can obtain the target sputtering rate.

Material transmission

As the sputtered particles move across the plasma, they collide with the neutral gas. The collisions slow some of the particles and backscatter others. In this section we derive a diffusion theory for computing the percentage of particles that reach the substrate. Such particles can be divided into two groups: those that reach the substrate and suffer only forward scattering, and those that are backscattered (scattered through an angle of $\pi/2$ radians or larger) and then diffuse to the substrate.

The derivation starts with the ideas and theory of G. Ecker and K. G. Emelens [11]. They present the problem of the sputtered particles diffusing to the substrate, but only for a linear subsonic diffusion (Fick- or Schottky-type diffusion). As will be seen, this subsonic diffusion is valid only for extremely high pressures.

K. B. Persson [12] presents a general theory of diffusion that goes farther than those commonly presented. It is valid for both supersonic and subsonic diffusion, and also for the creation and annihilation of particles; it is derived for a plasma of two components. In this paper, Persson's general diffusion theory is applied to the problem of sputtered material moving toward the substrate.

For this paper, "streaming" means supersonic diffusion, i.e., diffusion in which the average velocity is greater than the thermal or random velocity of the particles. "Diffusion" means subsonic diffusion, which is what is usually considered in diffusion theories.

To determine what percentage of the sputtered material reaches the substrate, we assume that the particles start from the target and stream toward the substrate. This assumption is supported by Stuart and Wehner's data [13],

which show that the particles have an average velocity about 1.5 times their Maxwellian thermal velocity. Their average velocity is reduced by collision, and some particles, after suffering large-angle collisions or multiple collisions, have zero net velocity toward the substrate. These particles, considered to be lost from the streaming, then diffuse to either the target or the substrate. The remaining streaming particles reach the substrate with a velocity equal to their thermal velocity. This is the normal boundary condition for a gaseous diffusion process. The "lost" particles produce a density gradient across the target-to-substrate spacing and thus set up a process of diffusion toward the target, the substrate, and the walls of the system. In simple terms, this theory accounts for scattering of the streaming particles and the diffusion of particles after scattering.

Why consider both streaming and diffusion? If we consider only streaming, we could account for no loss of particles except by annihilation. The particle velocity would always have to be no greater than the thermal velocity, and the particle density would be greatest at the substrate. If we considered only subsonic diffusion, we would meet the opposite limitations. No particles would reach the substrate without suffering large-angle collisions, and all the particles would have an average velocity smaller than their thermal velocity. This would contradict observations of velocity distributions at low pressure for both metal and SiO_2 targets [13, 14]. Hence, both streaming and diffusion must be considered.

To simplify the theory, the streaming and diffusion of particles to the wall will be taken into account by the geometric factor calculated by Schwartz, Jones, and Maissel [15]. This factor allows the diffusion analysis to be one-dimensional.

The derivation of the resultant equation for the percentage of sputtered material reaching the substrate is presented in Appendix B and is given by

$$\beta = \frac{M^*\lambda}{D}\left[1 - \exp\left(-\frac{D}{M^*\lambda}\right)\right], \qquad (2)$$

where D is the target-to-substrate spacing, λ is the mean free path of the material, and M^* is the mach number of the sputtered material at the target or at low pressures. Time-of-flight data indicate that $M^* \approx 1.5$. By curve-fitting this equation to experimental data, we found a $p\lambda$ value $\approx$ 8 Pa-cm (0.06 torr-cm).

Recently, F. Sequeda [16] has measured the sputtered particle density and deposition rates in the region of $pD \approx 30$ Pa-cm (0.25 torr-cm). W. D. Westwood [17] has also discussed sputtered material; however, it should be noted that the above λ is equivalent to his $\eta^1\lambda$. The value of 8 Pa-cm is still higher than that of Ref. [17], and is closer to the calculations in Ref. [18].

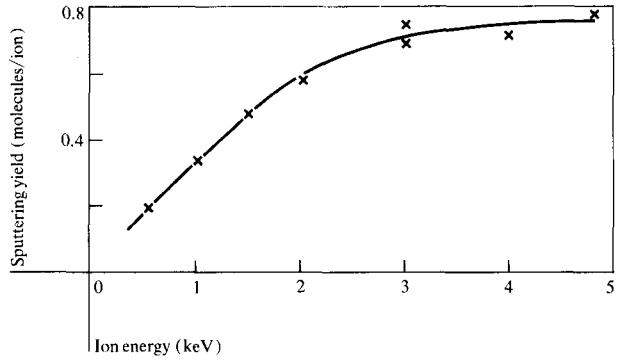

Figure 5 Sputtering yield in molecules per ion vs the ion energy. The standard deviation of the points is 0.03 molecules per ion or about five percent.

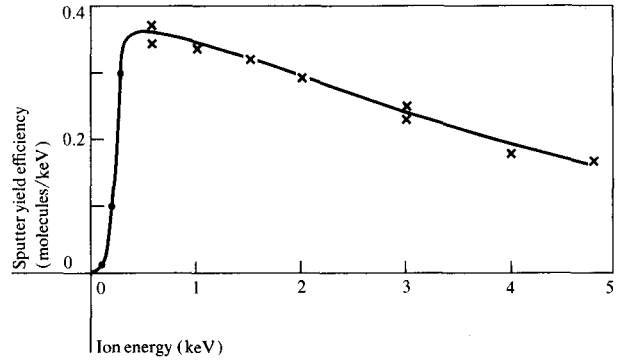

Figure 6 The yield efficiency (molecules/keV) vs the ion energy.

Re-emission coefficient and accumulation rate

At low pressure ($pD \approx 4$ Pa-cm, 0.03 torr-cm), the transmission of the sputtered material across the target-to-substrate spacing is nearly unity. In this case, the accumulation rate (incident rate minus the total re-emission rate) is nearly equal to the target yield times one minus the re-emission coefficient of the substrate. This expression is exact if the sticking coefficient of the target is unity. When the sputtering pressure is increased, however, the situation is complicated by the backscattering of material to both the substrate and the target.

To solve for the accumulation rate in terms of the target yield, pressure, and re-emission coefficients, the following definitions are made:

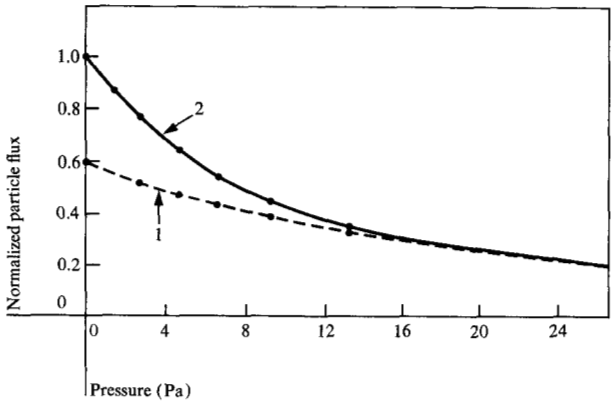

Figure 7 Normalized particle flux vs pressure for a target-to-substrate spacing D of 2.5 cm. Curve 1 shows the ratio of deposition rate to the sputter yield Y. Curve 2 shows the fraction of particle flux reaching the substrate. For these curves, $Y_s = 0.1Y$, $RE_t = 0.35$, $RE_s = 0.41$, and the temperature was 350°C.

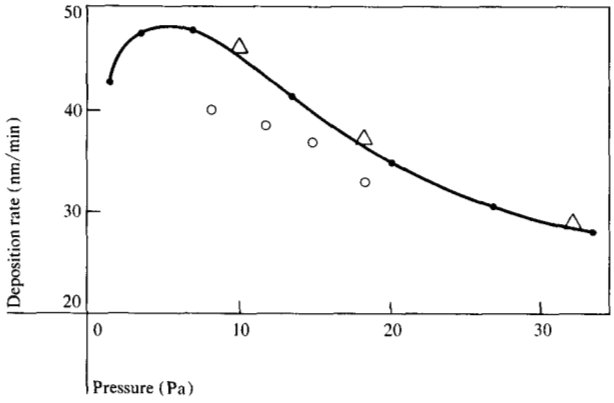

Figure 8 Deposition rate vs pressure. The curve represents the theoretical values, and the data points are those for two studies conducted in these laboratories by H. Koenig (△) and P. Huang (○).

deposition rate = accumulation rate

RE_s = reflection coefficient of the substrate

RE_t = reflection coefficient of the target

β = transmitting coefficient for the sputtered material (fraction of material that leaves the target and reaches the substrate)

α^* = total re-emission coefficient, i.e., the re-emitted material is equal to α^* times the total material incident on the substrate

Y = sputtering rate of the target, exclusive of RE_t

Y_s = sputtering rate of the substrate, exclusive of RE_s

We assume that Y and Y_s are due to energetic particles, as seen in the above sections. Thus, RE_s and RE_t are independent of target and substrate voltages. We also assume that RE_s and RE_t are functions of temperature T, and have used

$RE = a + bT$ for $100 < T < 500$°C;

β, Y, Y_s, RE_t, and RE_s are assumed to be independent of one another. To find the deposition rate and α^* as functions of Y, Y_s, β, RE_t, and RE_s, one can solve the simultaneous equations of emission, transmission, and reflection at the target, sputtering gas, and substrate. This is similar to solving for the transmitted light through three interfaces. The solution is given by

$$\text{Deposition rate} = \frac{Y\beta(1 - RE_s) - Y\beta(1 - RE_t)}{1 - (RE_s + RE_t)(1 - \beta) + RE_sRE_t(1 - 2\beta)}. \quad (3)$$

For SiO_2, it was assumed that $RE = 0.2 + 0.00058\ T$ (in °C). This is in fair agreement with the data published by Maissel et al. [19].

Equation (3) shows that if $\beta << 1$, i.e., if pD is greater than 8 Pa-cm (0.06 torr-cm), the functional dependencies are very complicated. If $\beta = 1$, Eq. (3) reduces to

$$\text{Deposition rate} = \frac{Y(1 - RE_s) - Y_s(1 - RE_t)}{1 - RE_sRE_t} = \frac{Y(1 - \alpha^*)}{1 - RE_sRE_t}. \quad (3a)$$

Figure 7 shows a plot of the ratio of the deposition rate to Y vs the pressure, where D is equal to 2.5 cm, $Y_s = 0.1\ Y$, $RE_s = 0.41$, $RE_t = 0.35$, and $T = 350$°C. Also shown (curve 2) is β, the percentage of particle flux reaching the substrate, vs pressure ($D = 2.5$ cm).

Discussion

Predicted and observed deposition rates are compared in Table 1. At present, the largest error in the program is believed to be due to the neglect of target-edge effects.

Figure 8 is a curve of the deposition rate vs pressure for a fixed spacing D of 2.5 cm. This curve shows the optimum pressure. Below the optimum, the target yield drops because the target voltage increases with decreasing pressure; above the optimum, the backscattering of the sputtered material reduces the deposition rate.

Figure 9 shows a logarithmic plot of deposition rate vs pressure for a spacing $D = 3d$ (d is the dark space thickness). When $D < 2$-$3d$, the sputtering plasma becomes unstable or is extinguished, and the resulting depositions are nonuniform. For curve 1, the target power density was held constant at 2.5 W/cm^2; by decreasing D as the pressure is increased, the optimum pressure increases to

Table 1 Comparison of predicted and observed deposition rates.

System	*Power* (kW)	*Pressure* (10^{-3} torr)	(Pa)	*Spacing D* (cm)	*Temperature* (°C)	*Deposition rate* (nm/min) *Observed*	*Predicted*	*Error in prediction*
Driven	0.93	10	1.3	2.5	250	35.6	41.0	+13
(out of	0.85	10	1.3	3.1	250	29.7	34.2	+13
phase)	0.95	40	5	3.1	250	32.0	38.4	+13
	0.95	40	5	3.1	70	38.0	42.4	+11
CARE	1.6	75	10	2.5	295	34.0	31.8	− 7
	2.4	75	10	2.5	370	50.0	47.5	− 5
	1.6	135	18	2.5	296	26.0	23.9	− 9
	2.4	135	18	2.5	370	41.0	39.4	− 4

about 10 Pa (0.08 torr). For both curves the phase of the substrate voltage was assumed to be similar to that of a controlled area ratio system (180 degrees). Curve 2 shows the deposition rate plotted vs pressure for a constant wafer temperature (350°C for a n^+-type wafer); the curve was obtained by computing wafer temperature as a function of power and pressure. Here, at low pressures, increases in the deposition rate are due to decreases in the target voltage; at higher pressures, increases are mainly due to increased gas cooling of the wafer, and thus attributable to increases in the target power.

APL program

This section describes the experimental APL program that calculates deposition rates for an arbitrary parallel plate sputtering system. The main program (or function) uses the above theory to calculate deposition rates for SiO_2. This program is applicable to magnetic as well as nonmagnetic systems, provided the target voltage is known for the system. It is an interactive program, which prompts the user for input and then calculates the predicted deposition rate. The predicted rate is for a clean system. If a system contains large amounts of water vapor (because of insufficient pump-down, leaks, or other sources of oxygen or oxygen radicals) the deposition rate may be substantially below that predicted by the program.

At present, if the target voltage is not known, the program will calculate a rough estimate of the target voltage for some nonmagnetic systems.

Perhaps the most important input required by the program, which is not always known, is the target power or the target power density. This is because the matching network losses may dissipate an appreciable part of the power that is input to the system. These losses are directly proportional to 1) the target voltage squared, 2) the capacitance between the target and the target shield, and 3) the rf resistance of the coil in the matching network.

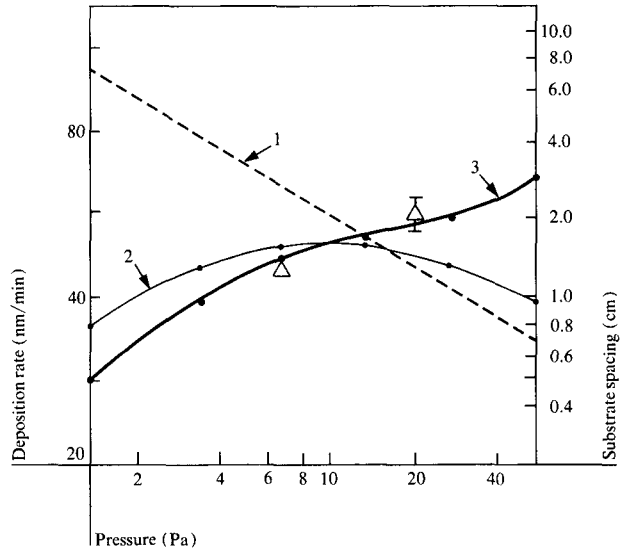

Figure 9 Logarithmic plot of the theoretically calculated (solid curves) and experimentally obtained (△) deposition rates for $D = 3d$ (see curve 1) where the phase of the substrate voltage was 180 degrees for a constant target power density of 2.5 W/cm^2 (curve 2), and for a constant wafer temperature, 350°C for a n^+-type wafer (curve 3).

Appendix A

This appendix gives the derivation of the energy distribution of the ions and energetic neutral species, due to charge exchange, that strike the target. The following assumptions are made in the derivation:

1. The cross section for ion collisions and charge exchange does not change with energy. The cross section for symmetrical charge exchange usually decreases with energy, but for the range of ion energies of interest, this decrease is sufficiently small.
2. The ions originate in the plasma; i.e., the percentage of ions that originate from ionization by electrons is

small. This assumption is fairly good for rf sputtering plasmas operated at pressures below 66 Pa (0.5 torr).

3. The electric field is constant across the sheath.

The third assumption greatly reduces the complexity for the fourth group of particles defined in the particle energy section. While the third assumption is not exact, the results of the derivation have been compared with the results of Davis et al. [20] for the ions; agreement within ±15% was obtained. This error is small compared to the error in the estimates of the mean free path, the errors due to the second assumption, and the estimate of the sheath thickness. Davis' results for the ions, in turn, show good agreement with experimental data.

With reference to the definition in the particle energy section, the number density and the energy density current distributions for the first group are

$$N(V)_1 = J_o \exp(-d/\lambda_i)\,\delta(V_o - V), \tag{A1}$$

$$E(V)_1 = J_o V_o \exp(-d/\lambda_i)\,\delta(V_o - V), \tag{A2}$$

where J_o is the number of ions entering the sheath per second, V_o is the dc bias across the sheath, d is the sheath thickness, and λ_i is the mean free path of the ions. For the second group,

$$N(V)_2 = \frac{dJ}{dV} = \left(\frac{dJ}{dx}\right)\frac{dx}{dV},$$

but

$$\frac{dJ}{dx} = \frac{J_o}{\lambda_i}\exp\left(-\frac{Vd}{V_o\lambda_i}\right),$$

and

$$\frac{dx}{dV} = \frac{d}{V_o}.$$

Thus,

$$N(V)_2 = \frac{dJ_o}{\lambda_i V_o}\exp\left(-\frac{Vd}{V_o\lambda_i}\right), \tag{A3}$$

and

$$E(V)_2 = \frac{VdJ_o}{V_o\lambda_i}\exp\left(-\frac{Vd}{V_o\lambda_i}\right). \tag{A4}$$

The third group is identical to the second, due to the constant electrical field assumption; thus,

$$N(V)_3 = N(V)_2 \tag{A5}$$

and

$$E(V)_3 = E(V)_2. \tag{A6}$$

The fourth group is composed of the particles that start from rest somewhere in the sheath and are accelerated to an energy V before suffering charge exchange. The number of particles per second is given by

$$N(V)_4 = \frac{J_o d}{V_o\lambda_i^2}\int_{\frac{Vd}{V_o}}^{d}\exp\left(-\frac{Vd}{V_o\lambda_i}\right)dx; \tag{A7}$$

$$N(V)_4 = \frac{J_o d^2}{\lambda_i^2}\left(1 - \frac{V}{V_o}\right)\exp\left(-\frac{Vd}{V_o\lambda_i}\right), \tag{A8}$$

and

$$E(V)_4 = \frac{J_o V d^2}{V_o\lambda_i^2}\left(1 - \frac{V}{V_o}\right)\exp\left(-\frac{Vd}{V_o\lambda_i}\right). \tag{A9}$$

Thus, the total energy distribution of the ions and neutral species striking the target is given by

$$E(V) = \frac{J_o Vd}{V_o\lambda_i}\left[2 - \frac{d}{\lambda_i}\left(1 - \frac{V}{V_o}\right)\right]\exp\left(-\frac{Vd}{V_o\lambda_i}\right) + J_o V_o\,\delta(V_o - V)\exp\left(-\frac{d}{\lambda_i}\right). \tag{1}$$

Appendix B

Diffusion of sputtered material

This appendix gives the derivation of the current of sputtered material that reaches the substrate as related to the material sputtered from a target.

Streaming The first part deals with the derivation of the particle current from a target that is only forward scattered as it crosses the space between the target and substrate, D. The analysis will be one-dimensional, as discussed in the diffusion section.

From the continuity equation,

$$\nabla \cdot nv = \frac{d}{dx}(nv) = -nv_i, \tag{B1}$$

where n is the streaming particle density, v is the average velocity, and ν_i is the rate at which particles are lost from the stream, i.e., the rate at which particles are backscattered.

From the momentum equation,

$$\frac{d}{dx}(\bar{M}nv^2) + \frac{d}{dx}(nkT) = -\bar{M}nv\nu_c, \tag{B2}$$

where $\bar{M}$ is the average mass of the streaming sputtered particles and ν_c is the collision frequency of the streaming particles. By using Eq. (B1), Eq. (B2) may be written as

$$\bar{M}nv\frac{dv}{dx} - \bar{M}nv\nu_i = n\frac{d(kT)}{dx} - kT\frac{dn}{dx} - \bar{M}nv\nu_c. \tag{B3}$$

In order to make Eqs. (B1) and (B3) a closed system of equations, we will assume that both kT and v are constants. These assumptions can be related to the following condition:

$$\left(1 - \frac{kT}{\bar{M}v^2}\right)\frac{dv}{dx} = \left(-\frac{1}{\bar{M}v}\right)\frac{d(kT)}{dx}. \tag{B4}$$

By using Eq. (B1) and the assumptions of constant kT and v, we get

$$-\bar{M}nv\nu_i = \frac{nkT\nu_i}{v} - \bar{M}nv\nu_c,$$

or

$$\left(1 + \frac{kT}{\bar{M}v^2}\right)\nu_i = \nu_c. \tag{B5}$$

From time-of-flight measurements,

$\bar{M}v^2 \approx 2kT$;

therefore,

$$\nu_i \approx \frac{2\nu_c}{3}. \tag{B6}$$

Use Eqs. (B1) and (B4) and integrate with respect to x to get

$$\Gamma_s = nv = \Gamma_o \exp\left(-\frac{2x}{3\lambda}\right), \tag{B7}$$

where Γ_o is the particle flux at the target and $\lambda = v/\nu_c$. Thus, the flux of the streaming particles Γ_s decreases exponentially with distance, as would be expected. The important feature of the derivation is that we now have a value of ν_i that is consistent with the exponential decrease of Γ_s.

Diffusion We can now write the continuity and momentum equations for the sputtered material that diffuses back to the substrate and target after being scattered out of the streaming flow. The continuity equation is

$$\frac{d}{dx}nv = +n_s\nu_i = \frac{2\Gamma_o}{3\lambda}\exp\left(-\frac{2x}{3\lambda}\right), \tag{B8}$$

where n and v now refer to the diffusion particle density and the average velocity, and n_s is the streaming particle density. Likewise, the momentum equation becomes

$$nv\frac{dv}{dx} + nv\nu_c + \frac{2v\Gamma_o}{3\lambda}\exp\left(-\frac{2x}{3\lambda}\right) = \left(-\frac{kT}{\bar{M}}\right)\frac{dn}{dx}. \tag{B9}$$

In theory, we can get the particle current due to diffusion, "Γ_d", by simply integrating Eq. (B8). This integration gives

$$\Gamma_d = nv = \int \frac{2\Gamma_o}{3\lambda}\exp\left(-\frac{2x}{3\lambda}\right)dx,$$

or

$$\Gamma_d = -\Gamma_o \exp\left(-\frac{2x}{3\lambda}\right) + C, \tag{B10}$$

where C is a function of λ and the spacing D between the target and substrate. The constant C determines the division of the particle current between the target and the substrate.

In order to find C, we can linearize Eqs. (B8) and (B9) and use the approximate boundary condition that $n = 0$ at the boundaries. Then Γ_d is

$$-D^*\frac{dn}{dx},$$

where the diffusion constant $D^* = kT/\bar{M}\nu_c$, and the constant C is thus defined. To make Eqs. (B8) and (B9) linear, we can make the normal diffusion assumption that $v^2 << kT/\bar{M}$. This assumption is fairly good except near the boundaries. By using $v^2 << kT/\bar{M}$, Eq. (B9) becomes

$$nv\nu_c = \left(-\frac{kT}{\bar{M}}\right)\frac{dn}{dx}. \tag{B11}$$

Taking the derivative with respect to x and using Eq. (B8), we obtain

$$\left(\frac{kT}{\bar{M}\nu_c}\right)\frac{dn^2}{dx^2} = -\frac{2\Gamma_o}{3\lambda}\exp\left(-\frac{2x}{3\lambda}\right).$$

Integration gives

$$\frac{nkT}{\bar{M}\nu_c} = -\frac{3\Gamma_o\lambda}{2}\exp\left(-\frac{2x}{3\lambda}\right) + C_1x + C_2.$$

By applying the boundary condition that $n = 0$ at $x = 0$ and at $x = D$, we get

$$\frac{nkT}{\bar{M}\nu_c} = -\frac{3\Gamma_o\lambda}{2}\left\{1 - \exp\left(-\frac{2x}{3\lambda}\right) - \frac{x}{D}\left[1 - \exp\left(-\frac{2D}{3\lambda}\right)\right]\right\}. \tag{B12}$$

By using $\Gamma_d = (kT/\bar{M}\nu_c)(dn/dx)$, Eq. (B12) becomes

$$\Gamma_d = -\Gamma_o\left\{\exp\left(-\frac{2x}{3\lambda}\right) - \frac{3\lambda}{2D}\left[1 - \exp\left(-\frac{2D}{3\lambda}\right)\right]\right\}. \tag{B13}$$

Thus

$$C = \frac{3\Gamma_o\lambda}{2D}\left[1 - \exp\left(-\frac{2D}{3\lambda}\right)\right],$$

and Eq. (B13) is consistent with Eq. (B10).

We can now find the total particle flux Γ_t by adding Eqs. (B13) and (B7); this gives

$$\Gamma_t = \frac{3\Gamma_o\lambda}{2D}\left[1 - \exp\left(-\frac{2D}{3\lambda}\right)\right]. \tag{B14}$$

References

1. P. D. Davidse and L. I. Maissel, "Dielectric Thin Films through RF Sputtering," *J. Appl. Phys.* **37,** 574 (1966).
2. P. D. Davidse and L. I. Maissel, "Rf Sputtering of Insulators," Third International Vacuum Congress, Stuttgart, Germany (1965).
3. P. D. Davidse, "Theory and Practice of RF Sputtering," *SCP Solid State Technol.* **9,** No. 12, 30 (1966).
4. P. D. Davidse and L. I. Maissel, "Equivalent DC Sputtering Yields of Insulators," *J. Vac. Sci. Technol.* **4,** 33 (1967).
5. H. Koenig, U.S. Patent 3,661,761, May 9, 1972.
6. J. S. Logan, "Control of RF Sputtered Film Properties through Substrate Tuning," *IBM J. Res. Develop.* **14,** 172 (1970).
7. J. L. Vossen, "Rf Sputter-etching and Sputtering with RF-induced Substrate Bias," *RCA Rev.* **29,** 566 (1968).
8. R. Auyang, K. Jaeckel, and J. S. Logan, "Power Network for Substrate," *IBM Tech. Disclosure Bull.* **14,** 1032 (1971).
9. H. R. Koenig and L. I. Maissel, "Application of RF Discharges to Sputtering," *IBM J. Res. Develop.* **14,** 168 (1970).
10. J. S. Logan, J. H. Keller, and R. G. Simmons, "The RF Glow Discharge Sputtering Model," *J. Vac. Sci. Technol.* **14,** 92 (1977).
11. G. Ecker and K. G. Emelens, "Cathode Sputtering in Glow Discharges," *Proc. Phys. Soc. London B* **67,** 544 (1954).
12. K. B. Persson, "Inertia-controlled Ambipolar Diffusion," *Phys. Fluids* **5,** 1625 (1962).
13. R. V. Stuart and G. K. Wehner, "Energy Distribution of Sputtered Cu Atoms," *J. Appl. Phys.* **135,** 1819 (1964).
14. B. Ryan, private communication, IBM Corporation, 3000 Westchester Ave., Harrison, NY.
15. G. C. Schwartz, R. E. Jones, and L. I. Maissel, "Distribution of Material Sputtered from a Disk Electrode," *J. Vac. Sci. Technol.* **6,** 351 (1969).
16. F. Sequeda, "Glow Discharge Optical Spectroscopy for Sputtering Diagnostics," Ph.D. Thesis, University of Illinois at Urbana-Champaign, Dept. of Metallurgy, 1978.
17. W. D. Westwood, "Calculation of Deposition Rates in Diode Sputtering Systems," *J. Vac. Sci. Technol.* **15,** 1 (1978).
18. F. J. Cadieu and N. Chencinski, "Selective Thermalization in Sputtering to Produce High T_c Films," *IEEE Trans. Magn.* **MAG-11,** 227 (1975).
19. L. I. Maissel, R. E. Jones, and C. L. Standley, "Re-emission of Sputtered SiO_2 during Growth and Its Relation to Film Quality," *IBM J. Res. Develop.* **14,** 176 (1970).
20. W. B. Davis and T. A. Vanderslice, "Ion Energies at the Cathode of a Glow Discharge," *Phys. Rev.* **131,** 219 (1963).

Received August 1, 1978; revised August 18, 1978

The authors are located at the IBM Data Systems Division laboratory, East Fishkill (Hopewell Junction), New York 12533.